Radio Science

RESEARCH ARTICLE
10.1029/2018RS006747

ICEBEAR: An All-Digital Bistatic Coded Continuous-Wave Radar for Studies of the *E* Region of the Ionosphere

Devin Huyghebaert[1], Glenn Hussey[1], Juha Vierinen[2], Kathryn McWilliams[1], and J.-P. St-Maurice[1]

[1]Department of Physics and Engineering Physics, University of Saskatchewan, Saskatoon, Saskatchewan, Canada, [2]Department of Physics and Technology, University of Tromsø, Tromsø, Norway

Key Points:
- A fully digital and remotely controlled radar installation named ICEBEAR with a bistatic setup is now operational
- ICEBEAR is the first continuous-wave spread-spectrum radar to measure ionospheric *E* region auroral irregularities
- ICEBEAR makes high spatiotemporal resolution images of auroral *E* region irregularities over a 600 km by 600 km field of view

Correspondence to:
D. Huyghebaert,
devin.huyghebaert@usask.ca

Citation:
Huyghebaert, D., Hussey, G., Vierinen, J., McWilliams, K., & St.-Maurice, J.-P. (2019). ICEBEAR: An all-digital bistatic coded continuous-wave radar for studies of the *E* region of the ionosphere. *Radio Science*, *54*, 349–364. https://doi.org/10.1029/2018RS006747

Received 19 OCT 2018
Accepted 17 MAR 2019
Accepted article online 15 APR 2019
Published online 30 APR 2019

Abstract The Ionospheric Continuous-wave *E* region Bistatic Experimental Auroral Radar (ICEBEAR) is a coherent scatter ionospheric radar. It operates at a frequency of 49.5 MHz, which is ideal for observing *E* region coherent echoes. The radar is located in Saskatchewan, Canada, and is operated by the University of Saskatchewan. The ICEBEAR system uses a continuous-wave (CW) signal and requires isolation between the receiving and transmitting arrays. This was accomplished through a bistatic setup, where the receiver and transmitter are ≈240 km apart. Currently, the ICEBEAR system implements a pseudo random noise phase modulation on this CW signal to obtain 3-km range resolution and 5-s integration time images of *E* region ionospheric irregularities over a 600 km × 600 km field of view. The center of the field of view is located at ≈58°N, 106°W. The radar design allows for future improvements to temporal and/or spatial resolutions. Each site consists of a linear phased array with 10 equally spaced antennas. This, combined with modern digital radio hardware, provides azimuthal angle of arrival measurements at the receiving array and azimuthal transmission control at the transmitting array. This publication describes the radio hardware and signal processing used by the ICEBEAR radar and emphasizes the unique capabilities of the radar. First ICEBEAR observations from a Kp ≥ 4 event on 10 March 2018, are presented and shown to produce simultaneously the four types of previously characterized *E* region coherent scatter echoes.

1. Introduction

Coherent scatter radars observe echoes from the ionosphere through the scattering of radio waves from naturally occurring large-amplitude plasma density perturbations generated by plasma instabilities. These perturbations are oriented along the magnetic field lines of the Earth, requiring the incident radio signal for a monostatic system to be approximately perpendicular to the geomagnetic field for radar scatter to occur (e.g., review by Fejer & Kelley, 1980). For a bistatic system, it is the bisector between the incident and scattered radio waves that must be perpendicular to the background magnetic field for scatter to occur (Haldoupis & Schlegel, 1993; Koehler et al., 1995). From the spectrum of the received signal one typically extracts a mean Doppler shift, a Doppler width, and a power level from the scattering region. Different types of coherent scatter radars have been used over the years to probe the *E* region, each radar having its own unique characteristics (e.g., Greenwald et al., 1995; Haldoupis & Schlegel, 1993; Koehler et al., 1995; Riggin et al., 1986).

Recent advances in radio technologies and techniques are allowing researchers to probe the ionosphere with increasingly higher accuracy and resolution and to localize the echo region with increasing precision. Some of these advances include improvements to analog to digital converters (ADCs), the ability to accurately synchronize multiple separately located system clocks, and the ability to generate transmission waveforms with increasingly more modulation control.

The enhanced accuracy and resolution provided by these advances is critical, as there are still many unanswered questions regarding *E* region scattering physics. Further investigations into the altitude dependence of *E* region radar measurement spectra and how the measurements of *E* region plasma irregularities vary with radar signal wavelength are needed. Reviews of the development of the understanding of *E* region radar measurements and attempts at answering some outstanding questions can be found in Fejer and Kelley (1980), Haldoupis (1989), Sahr and Fejer (1996), Schlegel (1996), Moorcroft (2002), Makarevich (2009), and Hysell (2016). These publications describe and characterize the different types of radar echoes received from

the ionospheric *E* region of the Earth and the technical progress that has taken place over the years. Recent progress has been made by St.-Maurice and Chau (2016) with regard to the generation and propagation of the plasma density irregularities in the *E* region. Some of these findings include the following: (1) The Doppler shifts observed close to the ion-acoustic speed in the vicinity of the $\mathbf{E} \times \mathbf{B}$ direction (so-called Type I) are from plasma density irregularities in the middle of the *E* region (near 110 km) because they are associated with the zero growth rates that the structures have when they reach their maximum amplitude; (2) the spectra with broad Doppler width and slow Doppler shifts in the vicinity of the electric field direction (so-called Type II) come from the fact that the structures are not plane waves but, instead, have a finite size along the electric field direction; (3) the narrow slow and narrow fast spectra (so-called Types III and IV) come from weakly growing structures at the top and the bottom of the *E* region plasma layer. A brief description of the different types of *E* region radar echoes are described in the next section.

1.1. *E* Region Coherent Scatter Spectra

To help quantify and understand the physics of the radar measurements, the observed Doppler spectra were separated into four different types by previous researchers (e.g., Sahr & Fejer, 1996). The types were classified by the spectral width and Doppler speed of the radar echoes. Type I echoes were observed to drift at approximately the ion-acoustic speed in a direction close to parallel with the electron $\mathbf{E} \times \mathbf{B}$ drift. Their spectral width was found to be measurably less than the mean Doppler shift of the echoes. Type I spectra were observed whenever the line of sight component of the electron drift exceeds the threshold speed of the Farley-Buneman instability (Buneman, 1963; Farley, 1963).

Type II echoes were observed to have a Doppler shift that is much smaller than the ion-acoustic speed and a spectral width on the order of the ion-acoustic speed. Based on equatorial electrojet observations, they were thought at first to be the bi-product of the gradient-drift instability (Fejer & Kelley, 1980; Knox, 1964; Reid, 1968; Tsuda et al., 1966). However, it has become evident that these Type II echoes are actually a nonlinear manifestation of Farley-Buneman instabilities when the observations are from a direction close to perpendicular to the background electron flow direction (e.g., Hamza & St.-Maurice, 1993; Otani & Oppenheim, 2006).

The rarer Type III and Type IV echoes were characterized by much smaller Doppler widths than Type I waves, to the point that they have been recently associated with weak turbulence (St.-Maurice & Chau, 2016). Type III echoes were observed to have Doppler shifts less than one half the ion-acoustic speed and were observed under strong Farley-Buneman instability conditions. It was therefore concluded that they are associated with the Farley-Buneman instability. Their recent detection at altitudes below 100 km by Chau and St.-Maurice (2016) has been shown to be consistent with the existence of weakly growing modes associated with Modulated Electron Ohmic Heating by Waves (Dimant & Sudan, 1997; St.-Maurice & Chau, 2016).

Type IV echoes were characterized by very narrow spectra and Doppler speeds significantly greater than (>2) the ion-acoustic speed. They are therefore thought of as being weakly growing modes (weakly turbulent) due to the narrow spectra. Similar to Type III echoes, Type IV echoes were observed under strong Farley-Buneman instability conditions. Various explanations for these spectra measurements have been suggested: Farley-Buneman waves growing in strongly unfavorable gradients (St.-Maurice et al., 1994), Farley-Buneman waves in the presence of high electron temperatures (Fejer et al., 1986), and weakly growing Farley-Buneman waves excited at the top of the *E* region layer, where the contribution of the ion motion added to that of the plasma density waves moving at the threshold ion-acoustic speed relative to the ions produces a Doppler shift that is comparable to the electron $\mathbf{E} \times \mathbf{B}$ drift for a ground-based observer (St.-Maurice & Chau, 2016).

1.2. Evolution in Radar Detection Techniques

The evolution in our understanding of the spectral types and of what they imply for the *E* region has advanced concurrently with the evolution and deployment of various coherent scatter radar techniques. For instance, CW observations performed by Prikryl et al. (1988, 1990) guided St.-Maurice and Hamza (2001) toward a description of the observed structures in terms of individual elongated structures that could be shown to slow down as they grew in amplitude. In general, CW measurements are rare for ionospheric radars but are extremely useful in that they can be used to continuously measure the evolution of ionospheric density structures, though this was typically at the expense of range resolution. To determine the range information of the radar scatter, traditionally pulsed radars were used.

Pulsed radar techniques have greatly improved through interferometry to the point of identifying the evolution of scattering centers as they moved through the radar field of view. An experimental setup by Hysell et al. (2012) used a coherent *E* region imaging radar array to probe the auroral ionosphere. It was proposed that a combination of the spectral width and the radar line of sight information in Type I and Type II waves could be used to produce a map of the electric field responsible for the growth of the unstable structures. This pulsed radar system operated at 30 MHz, obtained a range resolution of 2.25 km and a temporal resolution of 5 s, and the Doppler aliased at ±625 m/s.

Another coherent scatter radar in Kühlungsborn, Germany, measured ionospheric *E* region echoes with an experiment initially designed for meteor echoes during the St Patrick storm of 17 March 2015 (Chau & St.-Maurice, 2016). This multilink pulsed radar system obtained measurements at 36.2 and 32.55 MHz, with a temporal resolution of 10 s and a range resolution of 1.5 km. The angle of arrival in elevation and azimuth was able to be deduced through the use of a 2-D interferometer, where the range aliased every 240 km due to the interpulse period used. It was from this setup that the notion that Type III and Type IV echoes came from the lowest and highest altitudes of the unstable layer was developed. This, and the very narrow spectral widths of the scatter, triggered new theoretical ideas about the origin of these spectral types by St.-Maurice and Chau (2016).

It has also been shown that a passive CW technique can be applied to ionospheric measurements using FM radio stations as the transmitter sources (Lind et al., 1999, 2013; Sahr & Lind, 1997). Using an external radio signal source as the transmitter is known as "passive radar" and has the benefit of only requiring a receiver to make ionospheric measurements. Depending on the radio signal source, it is possible for this technique to have high spatial and temporal resolutions. Passive radars are typically bistatic as they operate using an external, uncontrolled transmission source. The spatial resolution of passive radars is dependent on the bandwidth (BW) used by the external radio source and is therefore not controllable by the radar user. This may result in differing spatial resolutions over time, thus making consistent measurements difficult. With a user-controlled radio transmission source (no longer a passive radar), it is possible to make consistent measurements.

Vierinen et al. (2016) have shown that it is possible to obtain high-resolution measurements of ionized meteor trails using a phase-modulated continuous-wave (CW) radio signal with a 30-W transmitter. The phase modulation consisted of transmitting a binary phase code with a set baud length. The radar obtained a range resolution of 1.5 km and operated at a frequency of 32.55 MHz. This low-powered, phase-modulated CW radar was shown to provide similar results to pulsed meteor radars operating at much higher peak powers. There have also been low-latitude experiments using low-power HF CW phase-modulated radars to measure the *F* region of the ionosphere that has shown promising results for this CW phase modulation technique (Hysell et al., 2016).

1.3. The ICEBEAR Radar

Utilizing a combination of the previously discussed modern radar techniques, a new *E* region coherent scatter radar system has been developed to provide enhanced measurements to further the understanding of auroral *E* region dynamics. This new radar is known as the Ionospheric Continuous-wave *E* region Bistatic Experimental Auroral Radar (ICEBEAR). ICEBEAR is located in Saskatchewan (SK), Canada, and observes the *E* region in the auroral zone perpendicular, or near perpendicular, to the magnetic field direction. ICEBEAR operates at very high frequencies (49.5 MHz) and utilizes the CW phase-modulated signal technique. A CW signal requires isolation between the transmitting and receiving antennas, or the transmitter signal will saturate the receiver. Due to this requirement the ICEBEAR transmitter and receiver sites are located approximately 240 km apart, though this is not necessarily the minimum separation distance for sufficient isolation. The minimum separation distance was not determined for ICEBEAR.

The ICEBEAR transmitter array consists of 10 antennas, and each antenna signal chain is controlled independently. The transmitter antenna signal chains are time synchronized and phase matched, allowing the array to operate as a digitally controlled phased array. In each transmitter chain there is a signal generator, power amplification, matched cables, and an antenna. Similarly, the ICEBEAR receiver array consists of 10 antennas and each receiver antenna signal chain is sampled (and controlled) independently. As with the transmitter array, each receiver antenna signal chain is time synchronized and phase matched, providing a digitally steerable phased array. Each receiver signal chain consists of an antenna, cables, preamps, filters, and a direct digitization sampler. The ICEBEAR transmitter is located in the southwest portion of the

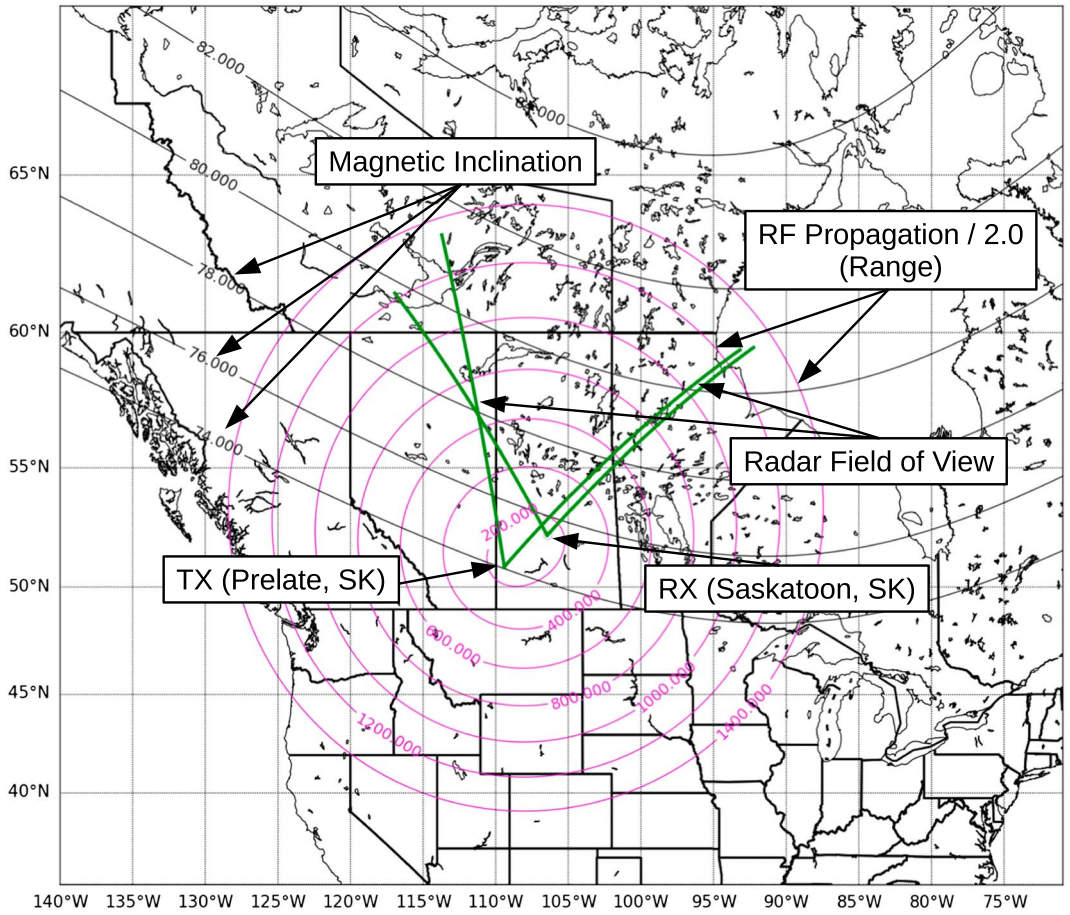

Figure 1. The locations and fields of view of the transmitter and receiver sites for the ICEBEAR radar. A zoomed-in version of this figure, with ionospheric scatter and the aspect angle at an altitude of 100 km, is shown later in Figure 7. ICEBEAR = Ionospheric Continuous-wave E-region Bi-static Experimental Auroral Radar.

province of Saskatchewan, near Prelate, SK, Canada (50.893°,−109.403°), and the receiver is located northeast of Saskatoon, SK, Canada (52.243°,−106.450°). Both sites can be remotely controlled and operated over the internet. A map of the site locations is presented in Figure 1.

The ICEBEAR receiver site was a previously established radar site close to the University of Saskatchewan. The transmitter site was selected for good overlap of the fields of view (FOVs) from the transmitter and receiving antenna arrays, which defines the ICEBEAR FOV. Other requirements for the ICEBEAR FOV were the field-aligned irregularity geometry (radio signal perpendicular to the geomagnetic field, also known as the magnetic aspect condition, for the required coherent plasma wave scattering conditions), and significant overlap with the Saskatoon Super Dual Auroral Radar Network (SuperDARN Greenwald et al., 1995) radar FOV for future collaborative studies. A note of significance regarding the FOVs shown in Figure 1 is that they are larger than expected from the antenna parameters given in the corresponding antenna specifications. This was verified through ionospheric scatter measurements at the edge of the shown FOVs, the location of which was determined through interferometry.

ICEBEAR uses CW phase modulation and interferometry techniques paired with modern radio hardware to obtain simultaneously high temporal and spatial resolution images of the *E* region over a large FOV while continuously sampling the ionospheric medium. These techniques remove aliasing in the frequency and range domains, although aliasing in the azimuthal and elevation domains must still be considered due to antenna spacing. Currently, both the Tx and Rx sites of ICEBEAR are set up with 10 antenna linear arrays with an equal antenna spacing of 6 m. There are plans to reconfigure the layout in the future to minimize or eliminate aliasing due to antenna spacing and also obtain elevation, along with nonaliased azimuthal, angle of arrival information. ICEBEAR operates with a center frequency of 49.5 MHz, providing a ≈1 wavelength

Table 1
ICEBEAR Amplifier Specifications

Characteristic	Goal	Result
Amplifier gain	60 dB	57 dB
Power output	60 dBm	59 dBm
Temperature monitoring	yes	yes
Fan monitoring	yes	yes
Output monitoring	yes	yes
Remote control	yes	yes
Rack mountable	yes	yes
Harmonics @ 50 MHz	best possible	26 dB down
Frequency span	2–50 MHz	20–50 MHz
Duty cycle	100% (CW)	100% (CW)

($\lambda = 6.06$ m) spacing between the antennas in the arrays. The 6-m spacing of the receiver array is due to a previous experiment setup, and the 6-m spacing of the transmitter array was chosen to match the receiver array.

The 10-antenna linear array with 1-wavelength spacing provides a beamwidth of $\approx 3°$. Grating lobes become significant when the beam is digitally steered to a point $\approx 30°$ off boresight. While this should not be a significant issue with the ICEBEAR radar, as the antennas chosen for the receiver and transmitter have beamwidths $\lesssim 52°$, it must be considered as results obtained through interferometry do appear in these regions at the edge of the FOV.

2. The ICEBEAR Transmitter System

The ICEBEAR transmitter site consists of an antenna array with a transmitter radar shed and associated radio electronics. This transmitter site is located near Prelate, SK, the location of which is indicated in Figure 1. The radar shed contains the power amplifiers, radio transceivers, and other associated electronics used for the control and generation of the ICEBEAR radar transmission signals, which are described in detail below.

The ICEBEAR transmitter site is situated on an abandoned farm yard, which had a preexisting electrical service. The preexisting connection reduced the costs and time associated with commissioning this new radar site. The transmitter site radar shed is a retrofitted shipping (sea) container, with heaters and an air exchange system to control the temperature. The coaxial feedline cables from the antennas connect to a bulkhead located on the transmitter shed, providing a method for implementing lightning protection. On the inside of the radar shed, this bulkhead has separate coaxial connections to each of the ICEBEAR power amplifiers. The site can be remotely controlled through a satellite internet connection, where the satellite dish is situated on the sea container roof.

2.1. The ICEBEAR Power Amplifiers

Part of the development of ICEBEAR included designing and building solid state linear CW power amplifiers. The amplifiers were designed with remote monitoring and control capabilities. To accomplish this a partnership with a local technology company, Scientific Instrumentation Ltd., was formed. Scientific Instrumentation Ltd. has expertise in electronics assembly and the design of electronics hardware enclosures, as well as construction of some scientific radars, such as the power amplifiers for the HF network of SuperDARN radars (Greenwald et al., 1995) and CADI ionosondes (MacDougall et al., 1995). The design goal for the amplifier output power was 1 kW, with minimal harmonics and signal distortion. On the monitoring side, there were requirements to be able to remotely monitor the temperature, fan speed, and output standing wave ratio (SWR) of the amplifier. The final specifications versus the goals are presented in Table 1. The specifications were all met, except for a slightly lower power output and gain of the power amplifier. An amplifier gain of 57 dB was achieved, with a CW power output of 59 dBm. When operated at 50 MHz, the third harmonic on the output was measured to be at least 26 dB below the peak signal power of 58 dBm, while the second harmonic was below the measurement range. The amplifier has operational frequencies

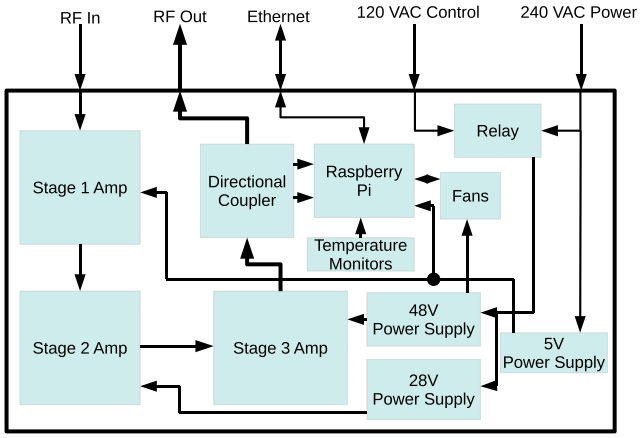

Figure 2. Block diagram of the power amplifier enclosure designed and built for the ICEBEAR transmitter system. ICEBEAR = Ionospheric Continuous-wave E-region Bi-static Experimental Auroral Radar; RF = radio frequency; VAC = volts alternating current.

in the range of 20–50 MHz. The amplifier monitoring systems were all successfully implemented within the amplifier enclosure, and the enclosure is rack mountable.

Figure 2 shows a block diagram of the ICEBEAR power amplifier. The amplifier has three stages where the first stage has a gain of 18 dB, the second stage has a gain of 23 dB, and the third stage has a gain of 16 dB. The output from the final stage is passed through a directional coupler, which allows for the forward and reverse signal to be measured using a logarithmic power measurement circuit. This circuit takes the radio frequency (RF) signal and converts it to a direct current (DC) voltage proportional to its logarithmic power. The monitoring circuit board has three functions: (1) it uses an ADC to convert the logarithmic amplifier DC voltage values to a digital signal, (2) it includes the electronic components required for temperature monitoring and, (3) it provides the circuitry to control and monitor the amplifier enclosure fans.

To communicate with the monitoring circuit, the general purpose input-output (GPIO) pins of a Raspberry Pi (Upton & Halfacree, 2012) were used. Temperature sensors measure the temperature of the heat sinks on the second and third stage amplifiers, as well as the air temperature at the intake of the amplifier enclosure. The second and third stage power supplies are located inside the amplifier enclosure and are controlled by the Raspberry Pi and an external network-controlled power distribution unit (PDU). The PDU supplies a 120-VAC (volts alternating current) control source to a relay inside the enclosure and, when a 120 VAC is applied, the relay engages the 240-VAC connection to the second and third stage amplifier power supplies. The first amplifier stage and the Raspberry Pi are always powered when connected to a 240-VAC power source. The design was implemented in this manor so the amplifier could be monitored and controlled remotely at all times. There is also an SMA (SubMiniature version A) coaxial connector output (not shown in Figure 2) on the front of the amplifier enclosure, which provides an output signal, at an attenuated level of approximately −70 dB, for sampling and testing. The ICEBEAR transmitter radar signal is supplied to each power amplifier through a coaxial cable connected to a signal generator, and this amplified signal is then sent via coaxial cables to RF connectors on an aluminum bulkhead. This bulkhead is well grounded with lightning protection incorporated.

2.2. The ICEBEAR Transmitter Radio Hardware

The undistorted amplification of generated radar waveforms is of extreme importance in a radar system, but the systems that generate the preamplified waveform are of equal importance. The ICEBEAR system is based around the use of the Ettus Research X300 Software Defined Radio Transceiver (Ettus & Braun, 2015). The X300 is an advanced radio transceiver that provides the ability to digitally mix radio signals, when either transmitting or receiving, through the use of a field programmable gate array (FPGA) while simultaneously allowing time synchronization between multiple transceiver units. The radio front end of the system is adaptable through the use of daughtercards, which provide analog filtering, mixing (if needed), and amplification of the radio signal. ICEBEAR uses the BasicRX and BasicTX daughtercards, which allow signals in the range of 0–250 MHz to be transmitted (Tx) and received (Rx). As each X300 transceiver has two transmitter and two receiver channels available, two BasicTX daughtercards were required for the front end of the X300s on the ICEBEAR transmitter.

The X300 hardware can be synchronized between multiple geographically separate radar sites using an external clock. In the case of the ICEBEAR system, the transmitter and receiver sites were synchronized using a Global Positioning System (GPS) clock and a clock distribution unit: the Fury GPSDO GPS-disciplined clock (Jackson Labs, 2018) for the GPS clock, and the Ettus Research Octoclock (Ettus Researchs, 2018) for the clock distribution unit. Specifically, synchronization between the sites is achieved by distributing the 10 MHz and pulse-per-second (PPS) signals synchonized by the GPS clocks to the X300s using phase delay matched coaxial cables and the octoclocks (Lewandowski et al., 1999). The common clock shared between transceivers makes each signal chain phase coherent. Combined with the fact that each transmitter signal chain is controlled independently, where each signal chain has its own amplifier and

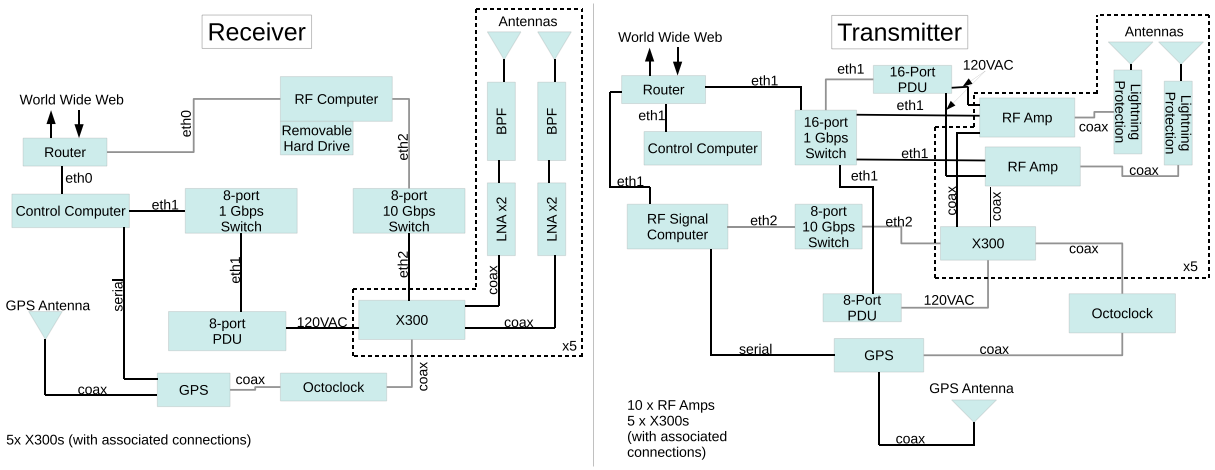

Figure 3. Block diagrams of the receiver and transmitter hardware, and the associated communication connections for the ICEBEAR radar. ICEBEAR = Ionospheric Continuous-wave E-region Bi-static Experimental Auroral Radar; RF = radio frequency; VAC = volts alternating current.

antenna, this allows for digital beamsteering and/or different transmissions on each antenna, providing the potential for unique experiments.

The accurate timing, provided by the GPS clock, of each RF complex voltage sample transmitted within the modulation scheme makes it possible to accurately determine the range of targets from which the radar signal scatters. In the case of the ICEBEAR system, the radar transmits a phase-modulated CW signal. By modulating the CW signal it is possible to obtain high temporal and high spatial resolution simultaneously while avoiding aliasing. The spatial resolution provided by the modulated CW signal is dependent on the bandwidth (BW) of the radio signal (Richards et al., 2010). The total propagation path resolution is given by

$$p_t = \frac{c}{BW}, \tag{1}$$

where p_t is the total path length, c is the speed of light, and BW is the bandwidth of the signal. For initial ICEBEAR operations, the transmitted signal had an effective BW of 100 kHz, providing a total path length resolution of 3 km. Total path length is the complete radio path length to and from the scattering region and is used instead of range due to the bistatic nature of the ICEBEAR system.

To generate a radio signal using an X300, a center frequency is selected and complex voltage samples are generated and streamed by the device. The hardware in the X300s has a maximum complex voltage sampling generation rate of 200 MHz on the RX and TX channels, with digital radio frequency up-converters and down-converters implemented on a FPGA for frequencies within this range. Higher sampling rates provide more control over the radar waveform characteristics, such as the radio BW, and allows for the implementation of digital signal filtering. The FPGA on an X300 digitally mixes the stream of complex voltage samples to the defined center frequency before transmitting the signal in the case of a transmitting configuration.

The current implementation of ICEBEAR uses an 800-kHz sampled complex voltage signal for transmission. This meets the necessary phase modulation rate of 100 kHz for a path length resolution of 3 km and also includes filtering of the signal to reduce side bands through the use of amplitude modulation to meet radio frequency licensing requirements. A sampling rate of 800 kHz was chosen as a compromise between excessive streaming bandwidth over ethernet to the X300s, and the need to accurately filter the signal. The filter used consisted of a running average of the signal to be transmitted, which is effectively a low-pass filter. The complex voltage sampling rate can be converted to a communication throughput data rate by recognizing that each complex voltage sample is a 32-bit complex number. For the 800-kHz sampling rate used by each ICEBEAR transmitter signal chain, there is a 25.6-Mb/s communication data rate per signal chain. This is the minimum data rate required between the transmitter host computer and an X300 for one transmission channel for the ICEBEAR configuration.

An overview of the complete ICEBEAR transmitter system is presented as a block diagram on the right side of Figure 3. One computer is needed for the overall control and generation of the transmitted waveform for

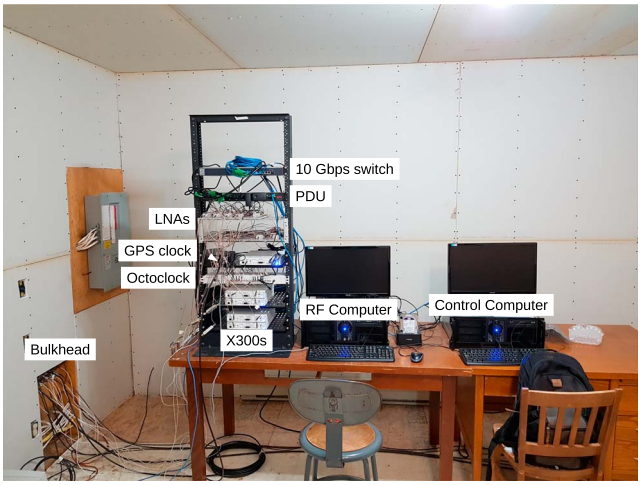

Figure 4. The ICEBEAR receiver electronics. On the electronics rack (on left) are the preamps, the X300s, the GPS clock, the Octoclock distribution unit, and the PDU. Directly to the right of the rack is the RF computer that controls the X300s and next to it is the monitoring control computer. There is an external HDD docking device next to the RF computer for transfer of data from the RF computer for later analysis. ICEBEAR = Ionospheric Continuous-wave E-region Bi-static Experimental Auroral Radar; GPS = Global Positioning System; PDU = power distribution unit; RF = radio frequency; HDD = hard disk drive.

the ICEBEAR transmitter (RF Signal Computer), while the other computer is used to monitor the transmitter amplifiers, the GPS clock synchronization, and to perform diagnostics on the overall radar site health (Control Computer). The computers operate using Ubuntu Linux (Thomas, 2006). On the RF Signal Computer, the GNURadio (Blossom, 2004) software suite and the USRP Hardware Driver (Ettus & Braun, 2015) are used to interface with the X300s. A 10-Gbps ethernet connection between the RF Signal Computer and a 10-Gbps switch is used to communicate with the five X300 transceivers (two channels per transceiver) on the same network. The 10-Gbps connection provides a large communication-BW connection to the X300s giving the capability to transmit high sampling rate generated radio signals.

The antennas used in the ICEBEAR transmitter array are Cushcraft 50-5 antennas (Cushcraft, 2018), which are five-element antennas designed for use in the 50-MHz amateur radio band. These antennas are different from those at the previously established receiver site. This was decided upon due to the Cushcraft 50-5 antennas being easier to assemble, having a broader beamwidth, and being easier to hoist when situated on the radar towers. The antennas were tuned to 49.5 MHz—the center frequency used with the ICEBEAR system—and provide a signal gain of 10.5 dBi with a maximum power capability of 1,000 W. Each antenna is mounted 15 m ($\approx 2.5\lambda$) above the ground on a tower and is located approximately 50 m from the radar shed. The antenna feedline consisted of 350 ft of DRF-400 coaxial cable which has an attenuation factor of 0.9 dB/100 ft at 50 MHz. The mounting height of the antennas produces a multilobe radiation pattern in elevation, with a peak at 4° elevation and a verticle beamwidth of ≈1.5°. This was determined through modeling and assuming an ideal ground plane. The phase delay along each transmitter signal chain was measured, allowing for digital phase corrections to the transmitted waveforms to be made, providing a fully coherent, and controllable, transmitter antenna array.

3. The ICEBEAR Receiver System

A great deal of the ICEBEAR TX system is mirrored by the ICEBEAR RX system, but there are some differences. As with the ICEBEAR TX system, the ICEBEAR RX system consists of a linear array of 10 antennas with 6-m spacing. The receiver site is located ≈240 km NE of the TX site and ≈20 km NE of the University of Saskatchewan in Saskatoon, SK, Canada. The receiver radar shed and antenna array existed from previous ionospheric radar experiments, and were repurposed and modified for use by the ICEBEAR radar. New ICEBEAR radar electronics were installed in the radar shed, and both the radar shed and antenna array were renovated. The new ICEBEAR electronics were necessary to achieve the high spatiotemporal observations and extract new and detailed information about the ionospheric plasma contained within the scattered radar signal.

3.1. The ICEBEAR Receiver Radio Hardware

A block diagram of the ICEBEAR receiver system is presented on the left side of Figure 3, with a photograph of the actual ICEBEAR receiver system hardware shown in Figure 4. The ICEBEAR receiver antennas are the Cushcraft 617-6B 6-m-wavelength Superboomer antennas with a forward gain of 16.15 dBi. These antennas are located ≈90 m north of the radar shed, are mounted 15 m above the ground, and are arranged as a linear array (for approximately east-west azimuthal interferometry). From each receiver antenna ≈600 ft of DRF-400 coaxial cable was used to connect to a bulkhead on the receiver radar shed. From the bulkhead each receiver antenna signal chain connects to a band-pass filter (BPF) and two low-noise amplifiers (LNAs) with 28-dB gain each. The BPF is required to attenuate nearby radio and TV signals and has a typical insertion loss of 6.1 dB. Signals at the antenna are therefore attenuated ≈12 dB before they are amplified at the LNAs (≈6-dB loss from feedline). This results in the system noise being slightly higher than the sky noise due to the LNA noise additions (≈2.9 dB per LNA), where the sky noise is typically 15 dB above that of the thermal noise generated by the antenna at 49.5 MHz (ITU-R, 2016). The LNAs are required to amplify the signal to be detectable by the receiver. Signals from the LNAs are transferred to the Ettus Research X300 transceivers,

where the received radar signal is directly digitized using the BasicRX daughtercards as the front end on the transceiver. The phase delay along each receiver signal chain has been characterized and is corrected for in software. The X300s communicate with the RF computer through a 10-Gbps switch, where the directly digitized radio signals are written to a hard disk drive (HDD).

The ICEBEAR RX computers operate using Ubuntu Linux. The Control Computer monitors the site and GPS lock, while the RF Computer receives a stream of radio samples from the X300s and records the data on a HDD. The RF Computer uses the GNURadio software suite and the USRP Hardware Driver driver to interface with the X300s. To record the data, the MIT Haystack DigitalRF software suite is used (MIT Haystack, 2018). The DigitalRF software indexes the complex voltage data samples streamed from the X300s and saves the samples in files using the HDF5 format (The HDF Group, 1997). The HDF5 format is a platform-independent method of storing and accessing data efficiently and effectively. DigitalRF corrects for dropped data samples and also records metadata for any given experiment. The voltage samples are stored on a local HDD on the RF Computer and transferred to an external HDD for transport to the University of Saskatchewan for analysis.

The X300 transceivers have a minimum sampling rate of 200 kHz in receiving mode, and this exceeds the current BW requirement of 100 kHz for 3-km path length resolution. Each of the 10 receiver signal chains have the raw complex voltage data individually recorded and saved on a HDD. The data rate resulting from this 10 receiver signal chain setup is 8 MB/s, or ≈700 GB/day if run continuously. After saving the data, postrecording beamforming and analysis can be performed on the raw complex voltages. Although keeping the raw complex voltage samples has large data storage requirements, it allows for variable time scale integrations and beamforming techniques to be implemented on the data. These data storage requirements of 700 GB/day are somewhat excessive at the moment, but with the cost of data storage decreasing and the amount of data that can be stored on a single device increasing, it should be manageable to run ICEBEAR continuously in the future.

3.2. ICEBEAR Signal Processing

To describe the ICEBEAR signal processing, the modulation of the radar signal for nominal ICEBEAR operations must first be discussed. For the current normal operation configuration, ICEBEAR uses a CW phase-modulated radar signal with a symbol, or baud, length of 10 μs, which corresponds to a BW of 100 kHz. This provides a total path length resolution of 3 km, as calculated from equation (1). The pseudo-random noise (PRN) code generated for the transmission signal is 10,000 symbols long, resulting in a code length of 100 ms. Using coded sequences in radars is known as pulse-compression, and serves to increase the range resolution, and thereby bandwidth, of the radar signal. The increase in the bandwidth due to this pulse compression is why radars utilizing a coded signal are known as "spread-spectrum" radars (Kelley & Weber, 1985). One benefit of using this spread-spectrum technique is that the PRN phase code provides a point-like radar ambiguity function, that is, a point-like resolution in Doppler frequency and range space (e.g., Richards et al., 2010; Sulzer, 1989). The range resolution is dependent upon the symbol length, and the Doppler resolution is dependent upon the sampling time.

The PRN phase code is also resistant to noise and interference, as well as appearing as noise to other radio systems. Using a PRN code makes it possible to obtain measurements even in a noisy environment. Due to this characteristic, the PRN code allows multiple radar transmitters to make use of the same band, providing the capability for multidirection simultaneous measurements of a common volume at the same frequency. For the initial ICEBEAR operations, an optimal PRN code was not rigorously searched for, though most 10,000 length pseudo-random binary codes have very similar characteristics with regard to their peak-to-sidelobe ratio (≈27 dB).

The 100-ms code length value used is the typical temporal resolution of each ICEBEAR measurement before averaging to improve the signal-to-noise ratio (SNR). The measurements do not alias in the frequency domain until ±50 kHz, which corresponds to ≈ ±150 km/s and do not alias in the spatial domain until a range of ≈30,000 km. Signals scattered from ionospheric irregularities are expected within 2,000 km of the radar and within a Doppler shift range of ± 500 Hz, which means that aliasing is not expected in the frequency and range domains for the ICEBEAR radar system.

A large amount of signal processing is required on the ICEBEAR raw complex voltage data to obtain scattered signal parameters, such as the power, spectral width and Doppler velocity. With optimized analysis

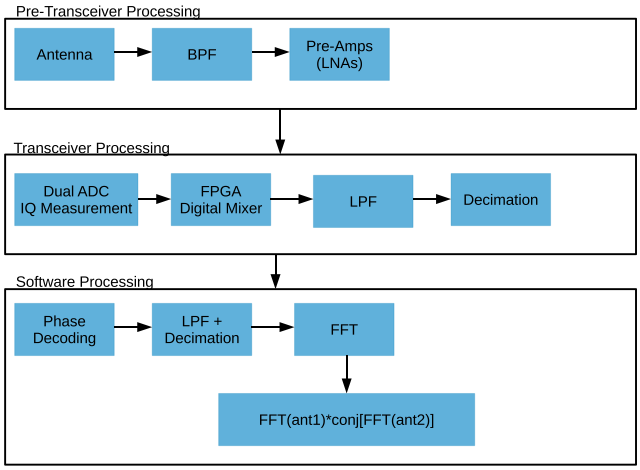

Figure 5. Block diagram of the processing of the radar signal, described in the text. BPF = band-pass filter; LNAs = low-noise amplifiers; ADC = analog to digital converter; IQ = in-phase and quadrature; FPGA = field programmable gate array; FFT = fast-Fourier transform.

code it was possible to achieve a processing time slightly faster than real time for two receiver signal chains (antennas) on a single Intel i7-7700 K cpu core. Processing the full array in real time could be accomplished using multiple cores and/or a graphics processing unit (GPU).

A block diagram of the hardware and software analysis processes are presented in Figure 5. The processing required to obtain the radar measurement spectral width, Doppler shift, and power may be divided into three steps: pretransceiver processing, transceiver processing, and software processing.

3.2.1. Pretransceiver Processing

For pretransceiver processing, the antenna acts as a BPF centered around 50 MHz, suppressing, but not eliminating, signals outside of the band. Once received at the antenna, the signal travels along 200 m of coaxial cable and is then filtered at the radar shed by a BPF, followed by two LNAs. After the BPF and LNAs, the signal is digitized by an X300 transceiver.

3.2.2. Transceiver Processing

For transceiver processing, each X300 transceiver is able to measure the RF signal from two signal chains at an ADC sampling rate of 200 MHz per chain. Each channel has a dual-ADC setup that provides the in-phase and quadrature (IQ) voltage samples of the respective RF signal chain at 200 MHz. The digitized signal is digitally mixed using the onboard FPGA in the X300 to the baseband (or DC) center frequency selected, which is 49.5 MHz for ICEBEAR. A digital low-pass filter and decimation stage is also implemented in the FPGA, reducing the data rates required to stream and record the signal. In the case of ICEBEAR the data are decimated from a data rate of 200 MHz to a data rate of 200 kHz.

3.2.3. Software Processing

The software processing stage extracts the physical quantities from the complex voltage sample data, which have been mixed, filtered, decimated, and stored from the previous transceiver processing stage. This is accomplished by decoding the phase of the received samples by multiplying them with the complex conjugate of the transmitted PRN phase code waveform (which is repeated every 10,000 samples), decimating the decoded signal, then finally converting to the frequency domain by performing a fast-Fourier transform (FFT) on the resulting samples, as described below.

For $N + r$ raw complex voltage samples given by an array,

$$V[t] = [V[0], V[1], \ldots, V[r+N-1]], \tag{2}$$

and the N sample complex code transmitted given by an array,

$$C[t] = [C[0], C[1], \ldots, C[N-1]], \tag{3}$$

one can then express the decoded voltage as a function of effective range and time as,

$$V_f[r,t] = \begin{bmatrix} V[0]C^*[0] & V[1]C^*[1] & \ldots & V[N-1]C^*[N-1] \\ V[1]C^*[0] & V[2]C^*[1] & \ldots & V[N]C^*[N-1] \\ \vdots & \vdots & \vdots & \vdots \\ V[r]C^*[0] & V[r+1]C^*[1] & \ldots & V[r+N-1]C^*[N-1] \end{bmatrix}, \tag{4}$$

where t is the samples in time, r is the largest range, and V_f is the decoded voltage as a function of range and sample (time) number. ICEBEAR operates with a PRN code of length $N = 10,000$.

Once the phase is decoded, each range has a voltage time series that is unique to that range. For ICEBEAR, after filtering, the samples are decimated from 200 kHz to 1 kHz, as this typically covers the range of Doppler frequencies expected and significantly reduces the FFT computation time. This provides a ±500-Hz Doppler range, corresponding to an ≈ ±1.5-km/s velocity range for the scatter. A FFT is calculated at each range, which produces a range-Doppler-intensity (RDI) spectrum for a given time for one antenna. The FFT also contains the phase information of each range-Doppler bin. The phase data are used for interferometry with

two or more antenna signal chains. For a 100-ms scan, the Doppler resolution is 10 Hz, while the processed RF propagation distance (total path length) resolution is determined by the receiver sampling rate, given by the equation

$$\Delta r = \frac{c}{f_s}, \tag{5}$$

where Δr is the RF propagation distance resolution, c is the speed of light, and f_s is the sampling rate. Note that the path length resolution of the radar is based on the baud length of the waveform transmitted, not the receiver sampling rate. If a radar signal is oversampled, it will appear to have a higher range resolution than is possible from the transmitted waveform.

A cross-correlation is performed between the range-Doppler bins of one antenna and the corresponding complex conjugate of the range-Doppler bins from another antenna. For two antenna signal chains, 1 and 2, this is given as,

$$S_{1-2}[r, f] = S_{\text{ant1}}[r, f] * S^*_{\text{ant2}}[r, f], \tag{6}$$

where S_{1-2} is the cross-spectrum between antenna 1 and 2, $S_{\text{ant1}}(r,f)$ is the range-Doppler spectrum of antenna 1, and $S^*_{\text{ant2}}(r, f)$ is the complex conjugate range-Doppler spectrum of antenna 2. From the cross-spectrum it is possible to determine the phase difference of a signal between two antennas at a given frequency.

Consecutive cross spectra were averaged over time to suppress the variance of the noise in the measurements. At this time the analysis involves fifty 100-ms ICEBEAR scans that are averaged to provide a time resolution of 5 s. The data can be reprocessed using fewer (or more) cross spectra in the averaging to study the evolution and decay of plasma irregularities in higher (lower) temporal resolution, but this is for future analysis. The analysis presented here provides a total path length resolution of 1.5 km, with the signal being sampled at 200 kHz, though the effective path length resolution is 3 km due to the transmitter waveform used. It should also be highlighted that meteor trails have been detected regularly with no averaging in single 100-ms observations, showing that measurements are possible with finer than 5-s temporal resolution.

Along with the range and temporal information provided by ICEBEAR, it is also possible to obtain azimuthal interferometry information through the use of the multiple antennas in the receiving array (Richards et al., 2010). This is accomplished by using the phase difference between the antennas of the received signal to obtain an angle of arrival, which is expressed as follows,

$$\sin\theta = \frac{\Delta\phi\lambda}{2\pi d}, \tag{7}$$

where θ is the angle of arrival, $\Delta\phi$ is the phase difference between antennas, λ is the wavelength, and d is the distance between the antennas. Calculating the angle of arrival using this method assumes that the received signal was a plane wave. The antennas are spaced at 1-wavelength intervals, so phase “wrapping" must be considered when determining the angle of arrival. This phase wrapping occurs at angles of arrival outside of $\pm 30°$ from the boresight of the array. Such situations will result in measurements appearing in the FOV, though originating from outside of it. For the geometry in this experiment, the location of scatter would have to be at large aspect angles for this to be a significant issue. Scatter at these large aspect angles are not expected due to the previous ionospheric scatter work referenced in section 1. The determination of the azimuthal angle of arrival, along with the range, of the scatter for each Doppler bin makes it possible to map the scatter source locations, providing details of the ionospheric plasma dynamics over a large FOV. An example of one of these maps can be found in section 5.

4. The ICEBEAR Experiment

The ICEBEAR radar first started operating in December 2017 and has been operating on a campaign basis subsequently. The experiment details of these first operations are given in Table 2. ICEBEAR has typically been operated when the Kp index is predicted to exceed 4, an indicator of likely magnetospheric activity (Thomsen, 2004). As data management and data analysis are more fully developed, ICEBEAR will be operated more often, with the goal of continuous operation for collaborative research.

Table 2
Specifications for Initial ICEBEAR Operations

Specification @ 49.5 MHz	Value
RX location	52.24319°,−106.450191°
RX pointing dir	7° East of North
TX location	50.893467°,−109.403151°
TX pointing dir	16° east of north
Transmitter peak power	300 W
Antenna spacing	1λ (6 m)
Modulation type	Binary PSK
TX symbol length	10 μs
TX path length resolution	3.0 km
RX sampling rate	200 kHz
CW modulation code length	10,000 samples
Range aliasing	30,000 km
Frequency aliasing	±100 kHz
Sample size	32-bit IQ
Data rate (10 RX)	8 MB/s

The first operations of the ICEBEAR system used four transmitters operating at 300 W at a center frequency of 49.5 MHz. Each of the transmitters transmitted the same pseudo-random code, with no phase shift applied. This resulted in 150 W after attenuation from the coaxial cable radiated from each of the four antennas. As each transmitter antenna has a gain of ≈10 dB, this provides a 1.5-kW effective radiated signal power (ERP) at each antenna. The value of 1.5-kW ERP per antenna assumes the antennas are 100% efficient and a SWR of 1.0, which is rarely the case. The antenna array gain factor has also not been included, but would increase the calculated ERP of the transmission and narrow the beam. At this output power there have been no issues obtaining ICEBEAR observations of *E* region plasma irregularities.

As mentioned in section 3.2, a PRN binary phase code was transmitted using phase modulation, also known as phase shift keying (PSK) in communications theory, with a symbol length of 10 μs and a code length of 10,000. This resulted in a time of 100 ms for the complete code length, corresponding to the 100-ms temporal resolution for each processed scan. The 10 μs symbols were subsampled at 1.25 μs on the transmitter signal to allow for amplitude modulation of the signal to reduce sidebands. This was required to keep the signal within the 160-kHz BW allowed by the Radio License.

The bistatic nature of the ICEBEAR configuration makes operations and analysis more complicated than a monostatic system in some regard. The range is not simply proportional to the time delay divided by 2, but is instead dependent on where the scatter occurs within the FOV, with two propagation paths of typically unequal length from the transmitter to the scattering location and from the scattering location to the receiver. Also, depending on where the scatter occurs within the FOV, the wavelength of the plasma density irregularities from which the radar signal scatters from will vary slightly. This effect was described for the SAPPHIRE radar (Koehler et al., 1995) and the SESCAT radar (Haldoupis & Schlegel, 1993), including references therein. The effect is given by,

$$k_{\mathrm{ir}} = 2k_r \cos(\theta/2), \tag{8}$$

where $k_{\mathrm{ir}} = 2\pi/\lambda_{\mathrm{ir}}$ is the wave number of the irregularities, $k_r = 2\pi/\lambda_r$ is the wave number of the radar signal, and θ is the angle between the rays from the transmitter to the scattering volume and the scattering volume to the receiver.

For the ICEBEAR configuration, the bisector between the propagation paths from the transmitter to the scattering location and from the receiver to the scattering location varies, with the bisector angle near 0° on the eastward side of the FOV and ≈15° on the westward side of the FOV. This corresponds to ionospheric irregularity wavelengths between 3.03 and 3.14 m. The direction of the Doppler velocity will also slightly vary with different scattering locations, with the velocity vector pointing toward the bisector of the receiver

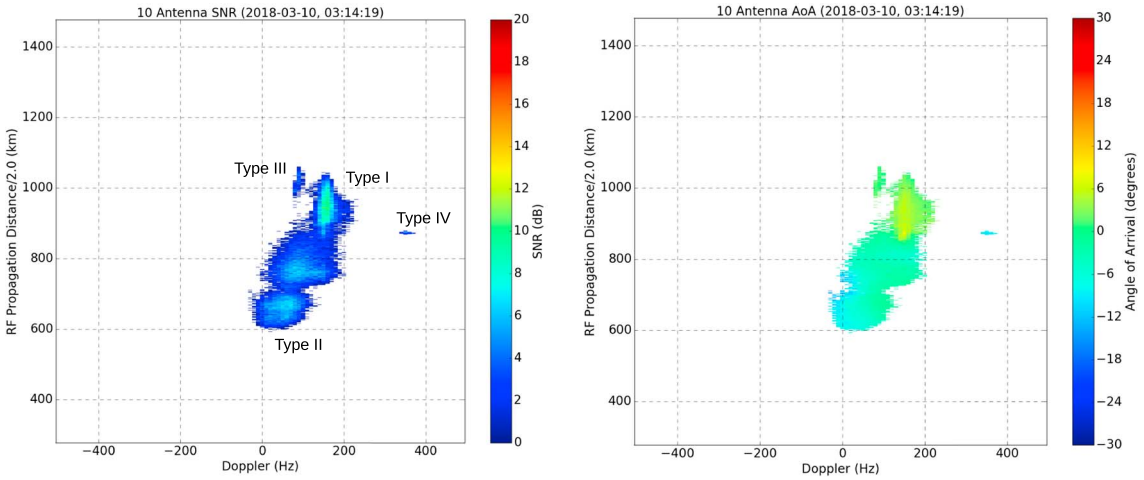

Figure 6. These plots show all four types of echoes in the same 5-s measurement. The SNR (left plot) is in decibel, with the bottom axis being the Doppler shift in frequency and the left axis the RF propagation distance divided by two. The angle of arrival calculated using 10 antennas for this event is displayed in the plot on the right, where the units are in degrees. The axes are the same as the SNR plot. Negative angle of arrival values are for scatter coming from the west, while positive ones are for scatter from the east. The measurement was taken on 10 March 2018, from 3:14:15 UTC to 3:14:20 UTC. This corresponds to a local time of 9:14 p.m. SNR = signal-to-noise ratio; RF = radio frequency; ICEBEAR = Ionospheric Continuous-wave E-region Bi-static Experimental Auroral Radar; AoA = angle of arrival.

and transmitter sites. At present, these wavelength and bisector variances are not taken into account, as they are small.

ICEBEAR data collected to date have provided an abundance of new, interesting, and highly detailed obervations. Some initial ICEBEAR observations will be presented in the next section.

5. ICEBEAR Results

From the cross spectra determined through the signal processing described in section 3.2, the Doppler frequency, power, spectral width, range, and angle of arrival (interferometry) of ionospheric radar scatter are available. During the day very little ionospheric scatter was detected, as is expected, other than meteor echoes. Ionospheric scatter is typically detected between local dusk and dawn, peaking around local magnetic midnight. 10 March 2018, was one date in particular that provided ionospheric scatter for over 9 hr, with all four types of *E* region radar echoes observed.

An example from this active day of a range-Doppler-intensity (RDI) plot is shown in the left plot in Figure 6. Figure 6 also shows the corresponding phase difference (interferometry) in the right plot. Data from all 10 receiver antennas were postreceive processed to generate Figures 6 and 7. Only data with a SNR greater than 1.0 (0.0 dB) were plotted, where the noise value was taken as the median value of the RDI spectrum, and each plot was a 50-scan average (5 s). All four types of *E* region radar echoes were observed simultaneously in Figure 6, but there is clearly more structure beyond the four types. From the interferometry data presented in Figure 6, the Type II echo (wide spectral width centered at ≈20 Hz) appears to be from the middle of the FOV and the Type I-like echo (strong echo at ≈150 Hz) is more to the east. Echoes from closer ranges have a Doppler shift closer to 0 Hz, while further range echoes tend to be moving toward the radar at greater velocities. A short-lived Type IV echo can be observed at a Doppler shift of ≈350 Hz, corresponding to a velocity of ≈1,050 m/s. There is also a Type III echo located at one of the further scatter ranges with a Doppler shift of ≈90 Hz.

Presenting the interferometry and Doppler velocity data together on a geographic map of the ICEBEAR FOV allows for the format presented in Figure 7. In this image the horizontal and vertical axes represent the longitude and latitude, respectively, the grayscale contour map represents the aspect angle at 100-km altitude (refraction was not considered), the magenta contour lines represent the total RF propagation distance divided by two, and the black contour lines represent the magnetic inclination. The green lines indicate the edges of the transmitter and receiver FOVs, and the color scale to the right represents the Doppler velocity of the scatter. The size of the velocity points are not scaled properly to azimuth, although they are scaled

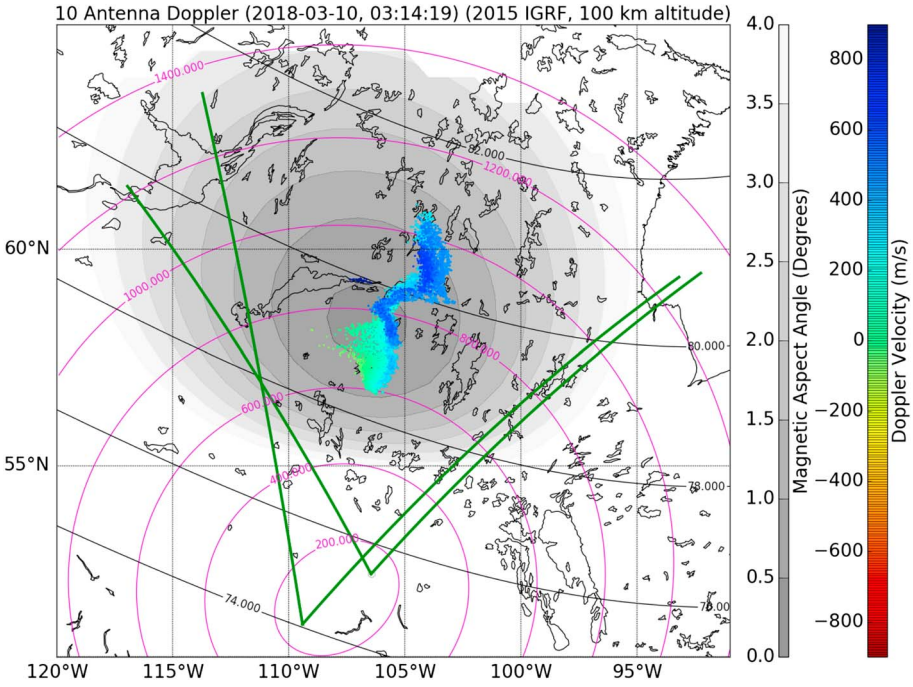

Figure 7. Plot of the ionospheric scatter mapped to geographic coordinates, which is described in the text. This plot corresponds to the same time as Figure 6. The Type IV echo is located at $\sim 59°N, 107°W$, immediately to the east of Lake Athabasca.

approximately correctly in range. The ionospheric scatter is very structured, with the Doppler properties of the scatter varying in both range and azimuth. Most of the scatter presents as a continuous distribution, except for the Type IV ionospheric scatter region which is clearly separated from the rest of the scatter. The Type IV echoes are located to the West of the other ionospheric scatter, at ≈107°W, 59°N, separated by a region of no scatter.

6. Conclusions

The ICEBEAR radar has been operational since December 2017. It is operating on a campaign basis during periods of high Kp. It uses a CW PRN phase-modulated signal to obtain high temporal and spatial resolution images of the *E* region, with a FOV over northern Saskatchewan in Canada. The use of a CW signal requires isolation between the receiver and transmitter antennas, resulting in the ICEBEAR transmitter and receiver sites being separated by ≈240 km. The phase modulation scheme used by ICEBEAR and the separation of the sites is only possible due to the implementation of modern radio hardware and techniques. Through the use of GPS-synchronized clocks and clock distribution units it is possible to operate multiple geographically separated radar sites and properly synchronize the radio samples. The Ettus Research X300 transceiver and Octoclock allow this synchronization to be implemented with relative ease. The X300 transceiver also allows the direct digitization of radio samples in the very high frequency range with no front end analog filtering and mixing. This, along with the advances in digital storage and computer processors, provides a means by which the raw voltage data can be stored and analyzed in close to real time.

For the initial ICEBEAR operations, the effective spatial resolution was 3 km, and the temporal resolution was 5 s. Both will be improved as the radar abilities are further explored, but the spatial resolution is constrained by Radio License BW limits, and the temporal resolution is constrained by requiring a sufficient SNR for detectable ionospheric scatter. Signal processing has currently been implemented for real time processing of two antennas, but is being expanded upon to make use of GPUs. By using a GPU it will be possible to process the 10 antennas of the receiving array in close to, or possibly faster than, real time.

The ICEBEAR radar has observed all four previously classified and measured *E* region radar echo types, as well as meteor echoes. Currently, the receiver and transmitter antennas are arranged as linear arrays providing angle of arrival in the azimuthal (east-west) direction through interferometry, though future research

plans include incorporating a 2-D array of antennas to obtain both azimuthal and elevation angle of arrival measurements.

Using the phase-modulated signal also allows multiple transmitting signals on the same frequency band. This is due to the PRN phase code appearing as noise when processed using a different code. With different codes transmitted at different locations by different transmitters, multiple measurements of the same ionospheric plasma volume may be obtained. These measurements could be used to produce 2-D or 3-D vectors of the plasma velocity to provide further insights into *E* region plasma dynamics and scattering physics.

Joint experiments with colocated instrumentation are planned in the future, with some attempts already having been made with the e-PoP satellite (Yau et al., 2006) and SuperDARN radars (Greenwald et al., 1995). Another instrument suite that will provide ample opportunity for collaboration is the Transition Region Explorer (TREx) installation, which is planned to have optical auroral imagery and total electron content (TEC) data over a significant portion of the ICEBEAR FOV (https://www.ucalgary.ca/aurora/projects/trex).

Every time the ICEBEAR radar is operated, new and exciting results are obtained. Multiinstrument studies of *E* region plasma dynamics with the ICEBEAR radar are expected soon, with meteor and potentially Alfvénic wave studies to follow in the future.

Acknowledgments
The authors would like to acknowledge the funding provided by the Canadian Foundation for Innovation (CFI), the Province of Saskatchewan, and the Natural Sciences and Engineering Research Council (NSERC) of Canada. The data used to generate Figures 6 and 7 are available at http://ion.usask.ca, where the transmission code as a binary file and the raw complex voltage data from each antenna in HDF5 format are available (Huyghebaert & Hussey, 2018). Unoptimized code written in python is provided with the data to generate the ICEBEAR spectra.

References

Blossom, E. (2004). GNU radio: Tools for exploring the radio frequency spectrum. *Linux journal*, *2004*(122), 4.
Buneman, O. (1963). Excitation of field aligned sound waves by electron streams. *Physical Review Letters*, *10*, 285–287. https://doi.org/10.1103/PhysRevLett.10.285
Chau, J., & St.-Maurice, J. P. (2016). Unusual 5 *E* region field-aligned irregularities observed from Northern Germany during the magnetic storm of 17 March 2015. *Journal of Geophysical Research: Space Physics*, *121*, 10,316–10,340. https://doi.org/10.1002/2016JA023104
Cushcraft (2018). A50-5S, www.cushcraftamateur.com
Dimant, Y., & Sudan, R. (1997). Physical nature of a new cross-field current-driven instability in the lower ionosphere. *Journal of Geophysical Research*, *102*(A2), 2551–2563. https://doi.org/10.1029/96JA03274
Ettus, M., & Braun, M. (2015). The universal software radio peripheral (USRP) family of low-cost SDRD. Opportunistic spectrum sharing and white space access: The practical reality, 3–23.
Ettus Researchs (2018). Octoclock www.ettus.com
Farley, D. T. (1963). Two-stream plasma instability as a source of irregularities in the ionosphere. *Physical Review Letters*, *10*, 279–282. https://doi.org/10.1103/PhysRevLett.10.279
Fejer, B., & Kelley, M. (1980). Ionospheric irregularities. *Reviews of Geophysics*, *18*(2), 401–454. https://doi.org/10.1029/RG018i002p00401
Fejer, B., Providakes, J., Farley, D., & Swartz, W. (1986). Auroral *E* region plasma waves and elevated electron temperatures. *Journal of Geophysical Research*, *91*(A12), 13,583–13,592. https://doi.org/10.1029/JA091iA12p13583
Greenwald, R. A., Baker, K. B., Dudeney, J. R., Pinnock, M., Jones, T. B., Thomas, E. C., & Yamagishi, H. (1995). DARN/SuperDARN. *Space Science Reviews*, *71*(1), 761–796. https://doi.org/10.1007/BF00751350
Haldoupis, C. (1989). A review on radio studies of auroral *E*-region ionospheric irregularities. *Annales Geophysicae*, *7*, 239–258.
Haldoupis, C., & Schlegel, K. (1993). A 50 MHz radio Doppler experiment for midlatitude *E* region coherent backscatter studies: System description and first results. *Radio Science*, *28*(6), 959–978. https://doi.org/10.1029/93RS01373
Hamza, A., & St.-Maurice, J. P. (1993). A turbulent theoretical framework for the study of current-driven *E* region irregularities at high latitudes: Basic derivation and application to gradient-free situations. *Journal of Geophysical Research*, *98*(A7), 11,587–11,599. https://doi.org/10.1029/92JA02836
Huyghebaert, D., & Hussey, G. (2018). 10 March, 2018, ICEBEAR Data—03:14:00-03:14:30 UTC, http://ion.usask.ca
Hysell, D. (2016). The radar aurora. *Auroral Dynamics and Space Weather, Geophysical Monograph*, *215*, 193–209.
Hysell, D., Miceli, R., Munk, J., Hampton, D., Heinselman, C., Nicolls, M., & Lessard, M. (2012). Comparing VHF coherent scatter from the radar aurora with incoherent scatter and all-sky auroral imagery. *Journal of Geophysical Research*, *117*, A10313. https://doi.org/10.1029/2012JA018010
Hysell, D., Milla, M., & Vierinen, J. (2016). A multistatic HF beacon network for ionospheric specification in the Peruvian sector. *Radio Science*, *51*, 392–401. https://doi.org/10.1002/2016RS005951
ITU-R (2016). Recommendation ITU-R P.372-13—Radio Noise, International Telecommunications Union.
Jackson Labs (2018). Fury GPS disciplined oscillator, www.jackson-labs.com
Kelley, K., & Weber, C. (1985). Principles of spread spectrum radar. In *MILCOM 1985—IEEE Military Communications Conference* (Vol. *3*, pp. 586–590). https://doi.org/10.1109/MILCOM.1985.4795104
Knox, F. (1964). A contribution to the theory of the production of field-aligned ionisation irregularities in the equatorial electrojet. *Journal of Atmospheric and Terrestrial Physics*, *26*(2), 239–249. https://doi.org/10.1016/0021-9169(64)90150-3
Koehler, J., Sofko, G., Andr, D., Maguire, M., Osterried, R., McKibben, M., & Ortlepp, A. (1995). The SAPPHIRE auroral radar system. *Canadian Journal of Physics*, *73*(3-4), 211–226. https://doi.org/10.1139/p95-029
Lewandowski, W., Azoubib, J., & Klepczynski, W. (1999). GPS: Primary tool for time transfer. *Proceedings of the IEEE*, *87*(1), 163–172. https://doi.org/10.1109/5.736348
Lind, F., Erickson, P., Coster, A., Foster, J., Marchese, J., Berkowitz, Z., & Sahr, J. (2013). Intercepted signals for ionospheric science. *Radio Science*, *48*, 248–264. https://doi.org/10.1002/rds.20034
Lind, F., Sahr, J., & Gidner, D. (1999). First passive radar observations of auroral *E*-region irregularities. *Geophysical Research Letters*, *26*(14), 2155–2158. https://doi.org/10.1029/1999GL900457
MIT Haystack (2018). Digital RF, https://github.com/MITHaystack/digital_rf
MacDougall, J., Grant, I., & Shen, X. (1995). The Canadian advanced digital ionosonde: Design and results. URSI INAG Ionospheric Station Inf. Bulletin, UAG-104.

Makarevich, R. (2009). Coherent radar measurements of the Doppler velocity in the auroral *E* region. *URSI Radio Science Bulletin*, *2009*(328), 33–46. https://doi.org/10.23919/URSIRSB.2009.7909539

Moorcroft, D. (2002). Outstanding issues in the theory of radar aurora: Evidence from the frequency dependence of spectral characteristics. *Journal of Geophysical Research*, *107*(A10), 1301. https://doi.org/10.1029/2001JA009218

Otani, N. F., & Oppenheim, M. (2006). Saturation of the Farley-Buneman instability via three-mode coupling. *Journal of Geophysical Research*, *111*, A03302. https://doi.org/10.1029/2005JA011215

Prikryl, P., André, D., Koehler, J., Sofko, G., & McKibben, M. (1990). Evidence of highly localized auroral scatterers from 50-MHz CW radar interferometry. *Planetary and Space Science*, *38*(7), 933–944. https://doi.org/10.1016/0032-0633(90)90060-4

Prikryl, P., André, D., Sofko, G., & Koehler, J. (1988). Doppler radar observations of harmonics of electrostatic ion cyclotron waves in the auroral ionosphere. *Journal of Geophysical Research*, *93*(A7), 7409–7424. https://doi.org/10.1029/JA093iA07p07409

Reid, G. (1968). The formation of small-scale irregularities in the ionosphere. *Journal of Geophysical Research*, *73*(5), 1627–1640. https://doi.org/10.1029/JA073i005p01627

Richards, M., Scheer, J., & Holm, W. (2010). *Principles of modern radar: Basic Principles*. Edison, NJ: Scitech Publishing.

Riggin, D., Swartz, W., Providakes, J., & Farley, D. (1986). Radar studies of long-wavelength waves associated with mid-latitude sporadic *E* layers. *Journal of Geophysical Research*, *91*(A7), 8011–8024. https://doi.org/10.1029/JA091iA07p08011

Sahr, J., & Fejer, B. (1996). Auroral electrojet plasma irregularity theory and experiment: A critical review of present understanding and future directions. *Journal of Geophysical Research*, *101*(A12), 26,893–26,909. https://doi.org/10.1029/96JA02404

Sahr, J., & Lind, F. (1997). The Manastash Ridge radar: A passive bistatic radar for upper atmospheric radio science. *Radio Science*, *32*(6), 2345–2358. https://doi.org/10.1029/97RS02454

Schlegel, K. (1996). Coherent backscatter from ionospheric *E*-region plasma irregularities. *Journal of Atmospheric and Terrestrial Physics*, *58*(8), 933–941. https://doi.org/10.1016/0021-9169(95)00124-7

St.-Maurice, J. P., & Chau, J. (2016). A theoretical framework for the changing spectral properties of meter-scale Farley-Buneman waves between 90 and 125 km altitudes. *Journal of Geophysical Research: Space Physics*, *121*, 10,341–10,366. https://doi.org/10.1002/2016JA023105

St.-Maurice, J. P., & Hamza, A. M. (2001). A new nonlinear approach to the theory of *E* region irregularities. *Journal of Geophysical Research*, *106*(A2), 1751–1759. https://doi.org/10.1029/2000JA000246

St.-Maurice, J. P., Prikryl, P., Danskin, D., Hamza, A., Sofko, G., Koehler, J., & Chen, J. (1994). On the origin of narrow non-ion-acoustic coherent radar spectra in the high-latitude *E* region. *Journal of Geophysical Research*, *99*(A4), 6447–6474. https://doi.org/10.1029/93JA02353

Sulzer, M. (1989). Recent incoherent scatter techniques. *Advances in Space Research*, *9*(5), 153–162. https://doi.org/10.1016/0273-1177(89)90353-0

The HDF Group (1997). Hierarchical data format, version 5., http://www.hdfgroup.org/HDF5/

Thomas, K. (2006). Beginning Ubuntu Linux: From novice to professional. Apress.

Thomsen, M. (2004). Why Kp is such a good measure of magnetospheric convection. *Space Weather*, *2*, S11004. https://doi.org/10.1029/2004SW000089

Tsuda, T., Sato, T., & Maeda, K. (1966). Formation of sporadic *E* layers at temperate latitudes due to vertical gradients of charge density. *Radio Science*, *1*(2), 212–225. https://doi.org/10.1002/rds196612212

Upton, E. , & Halfacree, G. (2012). *Raspberry Pi User Guide*. Chichester, UK: John Wiley & Sons Ltd.

Vierinen, J., Chau, J., Pfeffer, N., Clahsen, M., & Stober, G. (2016). Coded continuous wave meteor radar. *Atmospheric Measurement Techniques*, *9*(2), 829–839. https://doi.org/10.5194/amt-9-829-2016

Yau, A., James, G., & Liu, W. (2006). The Canadian Enhanced Polar Outflow Probe (e-POP) mission in ILWS. *Advances in Space Research*, *38*(8), 1870–1877. https://doi.org/10.1016/j.asr.2005.01.058